Available online at www.sciencedirect.com
SCIENCE DIRECT®
Journal of Magnetic Resonance 159 (2002) 111–125
JMR Journal of Magnetic Resonance
www.academicpress.com

Investigating hyperpolarized ^{129}Xe and CPMAS for spin polarization transfer to surface nuclei: a model study

Jay Smith,[1] Kevin Knagge, Luis J. Smith,[2] Ernesto MacNamara,[1] and Daniel Raftery*

H.C. Brown Laboratory, Department of Chemistry, Purdue University, West Lafayette, IN 47907, USA

Received 11 January 2002; revised 21 August 2002

Abstract

Several experimental techniques have been developed to utilize spin-polarized xenon gas for sensitivity and selectivity enhancement in surface studies using solid-state NMR. Although previously reported as a viable spin polarization transfer mechanism, the details of high-field cross-polarization (CP) have not been thoroughly investigated. We recently reported observations of CP from an adsorbed layer of hyperpolarized xenon (HP Xe) to a variety of surface nuclei at temperatures as high as 323 K [J. Am. Chem. Soc. 105 (2001) 1412]. In this paper, we investigate many of the issues associated with HP Xe surface CP studies, including polarization transfer kinetics and the effects of temperature on the dynamics. Protonated and methylated silica samples are used as model systems for comparison. A comparison of the rate analysis data from CP and SPINOE (Spin Polarization-Induced Nuclear Overhauser Effect) experiments provides information on the origin of the difference in polarization transfer efficiencies between the two techniques. Lineshape analysis of ^{1}H spectra for CP and SPINOE experiments demonstrates the difference in selectivity of methods due to longer SPINOE evolution times that lead to greater spin diffusion. The results of this work help to assess the viability of HP Xe CP as a surface analysis technique.

Keywords: Hyperpolarized xenon; Optical pumping; Solid-state NMR; CPMAS; SPINOE; Silica

1. Introduction

The functionality of many solid materials is determined, at least in part, by the chemical nature of the atoms at the heterogeneous interface between particles and their environment. The performance of zeolites, catalysts, coatings, and other such materials are often best characterized by the structure of the interfacial or surface atoms. Although there are many viable techniques for studying surface structure, NMR is potentially an ideal tool because it is non-destructive and chemically specific. However, the use of NMR in surface analysis requires overcoming two major obstacles, namely a lack of selectivity to the interfacial atoms and low sensitivity. To this end, hyperpolarized ^{129}Xe (HP Xe) [1–6] has been proposed as a mechanism for providing selective enhancement of the NMR sensitivity of only those atoms that come into intimate contact with the xenon [7–11]. HP Xe produced by optical pumping methods can attain spin polarizations as high as 10^5 times larger than thermal levels typically achieved in high magnetic fields and can serve as a large spin polarization reservoir for subsequent transfer to surface nuclei. And because it is chemically inert and adsorbs relatively strongly to many surfaces, HP xenon is a potentially ideal medium for polarization transfer. However, as will be discussed below, a number of challenges remain before the full potential of this method of polarization enhancement can be realized.

A number of techniques have been developed over the last decade to provide polarization transfer from HP Xe including low field thermal mixing, high-field cross-polarization, dissolution in liquid and supercritical xenon, and the spin polarization-induced nuclear

* Corresponding author. Fax: 1-765-494-0239.
E-mail address: raftery@purdue.edu (D. Raftery).
[1] Present Address: CNA Corporation, Alexandria, VA 22311, USA.
[2] Present Address: Argonne National Laboratory, Argonne, IL 60439, France.

1090-7807/02/$ - see front matter © 2002 Elsevier Science (USA). All rights reserved.
PII: S1090-7807(02)00015-0

Overhauser effect (SPINOE). Low field thermal mixing experiments provided the first successful demonstration of this methodology [7,8]. However, the necessity that the polarization transfer takes place outside the magnet makes subsequent use of high-resolution NMR challenging. Techniques based on dissolving samples in liquid [12,13] or supercritical xenon [14,15] can also produce sizeable signal enhancements however, issues of solubility and a loss of anisotropic information limits the applicability of these techniques to solid samples.

SPINOE has been demonstrated to provide sensitivity enhancements to nuclei in a variety of materials including liquid samples [10,16] and solid surfaces [17–23]. Perhaps most significant to surface studies, SPINOE has been shown to be amenable to a continuous flow of HP Xe under MAS conditions [18,19], allowing for signal averaging and resolution enhancement. Despite the fact that surface signal enhancements as large as 1200% have been reported, detailed analysis of the spin transfer kinetics have revealed that the extremely slow xenon/surface cross-relaxation rates ($10^{-3}\,s^{-1}$) require that surface nuclei have long T_1 relaxation rates (10^2–10^3 s) to achieve significant signal enhancement [24,25]. Also, the SPINOE enhancement drops dramatically with submonolayer xenon coverages and has not been observed at temperatures above 220 K for solid samples. Removal of fast relaxing nuclei that act as polarization sinks (protons, for example) can increase the enhancement of the method [24]; however, the strong dependence of the SPINOE enhancement on the T_1 relaxation time of the relevant surface nuclei limits the applicability of the experiment.

An alternative polarization transfer mechanism is high-field cross-polarization (CP). Like SPINOE, the CP experiment can incorporate a continuous xenon flow and magic angle spinning. Several studies have reported signal enhancements of surface protons by cross-polarization from an adsorbed layer HP Xe [9,23,26]. The conclusions drawn from much of the early work involving HP Xe CP indicated the experiment was limited to temperatures below 160 K, where xenon surface mobility is reduced. This view has been bolstered by studies using high pressures of thermally polarized xenon (up to 20 atm), which have reported CP sensitivity enhancements of xenon at high temperatures (near 298 K) from protons on surfaces with restricted xenon mobility [27–29]. Recently, we reported the observation of surface-sensitivity enhancement using HP Xe CP at temperatures as high as 323 K in systems where adsorbed xenon is relatively unconfined [30].

In light of the potential use of HP Xe CP experiments for surface-selective NMR studies, it is of interest to investigate the details of the CP process to surface nuclei. The purpose of this paper is to examine the CP transfer kinetics and temperature dynamics of two simple model systems and to determine the benefits and limitations of this technique as a surface analysis method compared to the more experimentally straightforward SPINOE method. As one might expect, the efficiency of cross-polarization transfer from adsorbed xenon to surface protons is determined by several temperature-dependent factors including the xenon surface coverage, correlation times for xenon lateral diffusion and adsorption, and the xenon and proton $T_{1\rho}$ relaxation times. This is complicated by the fact that the xenon surface polarization also changes with temperature. To get a better quantitative understanding of the limitations to the CP transfer mechanism, we studied the temperature dependence of many of these factors and their effect on the HP Xe CP to the surface protons of an M-5 Cab-O-Sil sample (Cabot Corporation, Boston, MA). Silica was selected as a model system for these studies because it has previously been well characterized by NMR [31], and methoxy studies were performed because the authors had previous experience with such systems [22,24,25].

2. Theory

The basic principles behind CP from an adsorbed layer of laser-polarized xenon to surface nuclei are the same as those found in a traditional CP experiment, but with a few differences in the details related to the dynamic nature of the spin-spin couplings. Although theoretically possible, J-coupling mediated polarization transfer is a seemingly unlikely mechanism due to low-coupling strengths predicted to be on the order of mHz–μHz [32]. This situation leads to the conclusion that the polarization transfer is mediated through dipolar coupling. At first, it might be somewhat difficult to imagine a dipolar coupling interaction between adsorbed xenon and surface protons that is not averaged to zero by the xenon mobility. The non-vanishing time-averaged dipolar coupling is simply due to the fact that the surface prohibits isotropic mobility of the adsorbed xenon and therefore, results in an incomplete averaging. A simple yet more mathematical argument supporting this claim can be made based purely on the geometry of the particle. For example, consider a thin layer of ^{129}Xe gas adsorbed on a proton containing surface. The particle size is assumed to be sufficiently large so as to limit xenon–proton couplings to only one side (2π steradians) of a given surface site. On the timescale of the xenon–proton coupling (>0.6 ms), the rapid surface mobility of the xenon allows individual pair-wise interactions with the surface protons to be replaced with a single average interaction having an effective internuclear vector lying parallel to the surface normal, as shown in Fig. 1. As-

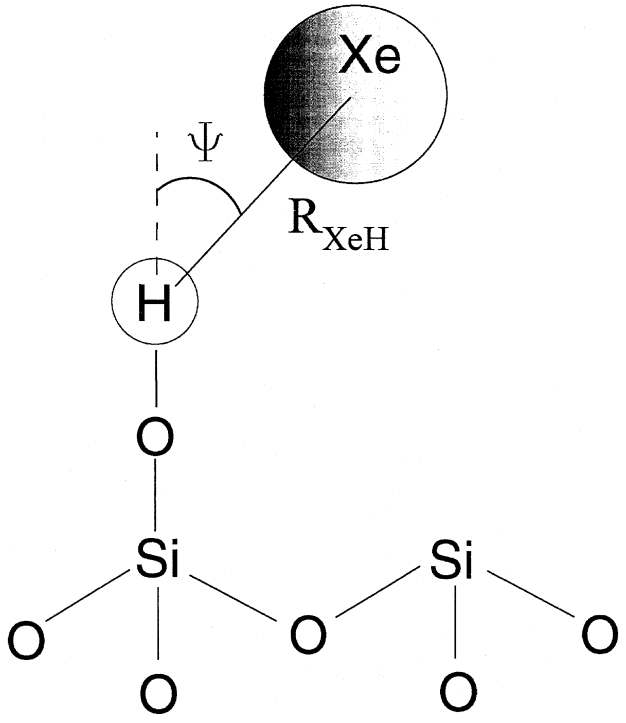

Fig. 1. Schematic diagram of the internuclear interaction between xenon and surface protons. R_{XeH} is the distance between nuclei and ψ is the angle between the internuclear vector and the surface normal.

suming a closest approach distance between the xenon and the surface of R_{Xe-H}, the time-averaged second moment of the dipolar coupling interaction using this model is simply

$$\langle M_2\rangle \propto \langle (3\cos^2(\psi_n)-1)^2\rangle_{\text{space}} \left\langle \frac{1}{r^6_{Xe-H}} \right\rangle_{\text{time}} \approx \frac{1}{10}\left(\frac{\hbar\gamma_{Xe}\gamma_H}{R^3_{Xe-H}}\right)^2 \theta'\delta_{\text{site}}R^2_{Xe-H}, \quad (1)$$

where ψ is the angle between the internuclear vector and the surface normal, r_{Xe-H} is the average distance between Xe and H nuclei, θ' is the coverage of ^{129}Xe, δ_{site} is the proton surface site density, and η is Planck's constant. Eq. (1) also includes an average over all possible orientations, ψ_n, of the surface normal. The second moment has all of the properties one would expect for this system, namely decreasing magnitude with decreasing xenon coverage, decreasing surface site density, or increasing nuclear size of the surface sites.

In general, cross-polarization can be pictured as a thermal equilibration process, where coupled spins approach a common spin temperature in respective rotating frames. Cast in terms of spin polarization enhancement $\xi = P/P_0$, where $P \equiv (N_\uparrow - N_\downarrow)/(N_\uparrow + N_\downarrow)$, the CP kinetics between a pair of spins (Xe and H) are described by a set of coupled differential equations of the form [33]

$$\begin{aligned}\frac{d\xi_{Xe}(\tau_{cntct})}{d\tau_{cntct}} &= -\left[\rho'_{1\rho Xe} + \varepsilon\sigma_{\rho XeH}\right]\xi_{Xe}(\tau_{cntct}) + \frac{\gamma_H}{\gamma_{Xe}}\varepsilon\sigma_{\rho XeH}\xi_H(\tau_{cntct}),\\ \frac{d\xi_H(\tau_{cntct})}{d\tau_{cntct}} &= \frac{\gamma_{Xe}}{\gamma_H}\sigma_{\rho XeH}\xi_{Xe}(\tau_{cntct}) - \left[\rho_{1\rho H} + \sigma_{\rho XeH}\right]\xi_H(\tau_{cntct}),\end{aligned} \quad (2)$$

where $\varepsilon = (N_H/N_{Xe})$ represents the ratio of surface protons to adsorbed xenon nuclei. ξ is closely related to η, defined by $(P–P_0)/P_0$, which is used to describe the polarization enhancement in the SPINOE experiments. The above equations assume strong, resonant B_1 fields are used to achieve the Hartmann–Hahn matching condition. The subscript "ρ" on the rate constants in Eq. (2) indicates that the rate information pertains to the rotating frame. The cross-polarization rate, $\sigma_{\rho XeH} = T^{-1}_{\rho XeH}$, is a measure of the coupling between the two spin systems and $\rho_{1\rho} = T^{-1}_{1\rho}$ accounts for spin-lattice relaxation. The primed notation on the xenon relaxation rate indicates an effective rate that is a combination of the true xenon relaxation rate, $\rho_{1\rho Xe}$, exchange kinetics with gas phase xenon, and the flow rate of the effluent xenon gas. In a more traditional spin system, CP occurs between neighboring nuclei and the ratio ε can be estimated from the number of nuclei surrounding a given site. Considering the mobility of xenon on the surface, on average each surface proton is in contact with a fraction of a xenon atom, which is determined by the coverage, θ. The ratio ε (equivalent to $1/\theta$) can be estimated from BET (Brunauer, Emmett, Teller) isotherm [34] coverage measurements and by making the assumption that the proton coverage is essentially 100%. The xenon coverage must also be scaled by the isotopic abundance of ^{129}Xe (26%), $\theta' = 0.26\theta$.

A couple of points need to be discussed regarding the spin temperature approximation. Typically in a CP experiment carried out under conditions where there is little mobility, the respective spin reservoirs can be described by a spin temperature, and the CP dynamics are well described by a thermodynamic picture [33]. In some cases, multiple, weakly coupled spin reservoirs are present, which can give rise to oscillations in the CP dynamics [35]. In our present situation, with the fast exchange of the xenon at the surface, we would expect that the xenon spin reservoir is at a common spin temperature. Similarly, surface protons that are in contact with the xenon are likely to be described by a single spin temperature. The dipolar coupling between these surface protons is sizable, and the mobility of the xenon itself helps to average out the individual Xe–H couplings. However, during the CP experiment, the spin temperature of these surface protons will likely be different than protons that do not come into contact with the HP xenon, and do not have the opportunity to contact the

surface protons via spin diffusion due to the limited CP time. This gives rise to a surface selectivity in the CP experiment (vide infra).

Using the boundary conditions $\xi_{Xe}(0) = \xi_{Xe}^{Surface}$ and $\xi_H(0) = 0$, the solutions to Eq. (2) for the HP Xe CP experiment have the form [33]

$$\xi_{Xe}(\tau_{cntct}) = \xi_{Xe}^{Surface}\frac{1}{2}\left[\left(\frac{r_-}{s}+1\right)e^{\lambda_+\tau_{cntct}} - \left(\frac{r_-}{s}-1\right)e^{\lambda_-\tau_{cntct}}\right],$$
$$\xi_H(\tau_{cntct}) = \xi_{Xe}^{Surface}\frac{\gamma_{Xe}}{\gamma_H}\frac{\sigma_{\rho XeH}}{s}\left[e^{\lambda_+\tau_{cntct}} - e^{\lambda_-\tau_{cntct}}\right], \quad (3)$$

with

$$r_\pm \equiv -\left[\rho'_{1\rho Xe} + \frac{\sigma_{\rho XeH}}{\theta'} \pm (\rho_{1\rho H} + \sigma_{\rho XeH})\right],$$
$$s = \sqrt{r_-^2 + 4\frac{\sigma_{\rho XeH}^2}{\theta'}}, \quad \text{and} \quad \lambda_\pm \equiv \frac{1}{2}[r_+ \pm s].$$

The utility of HP Xe CP as a surface analysis technique is best assessed in comparison to the more established SPINOE experiment. To understand the differences in the enhancements provided by these techniques, it is necessary to consider the spin polarization transfer kinetics for the SPINOE experiment, which is also under continuous flow conditions. The SPINOE experiment is described by the following set of coupled differential equations:

$$\frac{d\eta_{Xe}(t)}{dt} = -\rho'_{1Xe}\eta_{Xe}(t) + \frac{\gamma_H}{\gamma_{Xe}}\theta'\sigma_{XeH}\eta_H(t) + \rho^f\eta_{Xe}^{Cell},$$
$$\frac{d\eta_H(t)}{dt} = \frac{\gamma_{Xe}}{\gamma_H}\sigma_{XeH}\eta_{Xe}(t) - \rho_{1H}\eta_H(t), \quad (4)$$

that have been discussed in some detail in the literature [24,25]. It should be noted that in Eq. (4), we have explicitly taken into account the coverage dependence on the overall cross-relaxation rate, and we have defined η as the enhancement over the Boltzmann polarization, $\eta_I(t) = (I(t) - I_0)/I_0$. The SPINOE equations are very similar in form to those of CP (Eq. (2)), but with an additional term $\rho^f\eta_{Xe}^{Cell}$ to account for the introduction of new xenon gas from the pumping cell during the experiment. This is necessary due to the fact that the SPINOE experiments require much longer evolution times and do not take place in the rotating frame. In this study, we are not concerned with time dependence of the SPINOE enhancements, but rather the steady-state values. A reasonable approximation for the steady-state SPINOE enhancement can be obtained from Eq. (4)

$$\eta_H^{SS} = \frac{\gamma_{Xe}}{\gamma_H}\frac{\eta_{Xe}^{Cell}\rho^f}{\rho'_{1Xe}}\frac{\sigma_{XeH}\rho'_{1Xe}}{\rho_{1H}\rho'_{1Xe} - \theta'\sigma_{XeH}^2}$$
$$\approx \frac{\gamma_{Xe}}{\gamma_H}\theta'\eta_{Xe}^{Surface}\frac{\sigma_{XeH}}{\theta'\rho_{1H}}, \quad (5)$$

for the present experiments, where $\rho_{1H}\rho'_{1Xe} \gg \theta'\sigma_{XeH}^2$. It can be seen that the proton polarization enhancement depends on the surface xenon polarization, the proton relaxation rate, and the cross-relaxation rate. Alternatively, one can use the coverage-scaled cross-relaxation rate (as shown in Eq. (5)), which has a relatively flat temperature dependence [25] such that now it can be seen that the coverage is indeed a very important factor. The steady-state xenon enhancement is given by $\eta_{Xe}^{Surface} \equiv (\eta_{Xe}^{Cell}\rho^f)/\rho'_{1Xe}$.

Although the dynamics of the enhancements provided by CP are complicated, the overall enhancement relies heavily on the temperature dependence of the surface xenon coverage and polarization. According to Eq. (3), the CP enhancement achieves a maximum of

$$\xi_H^{max} = \xi_{Xe}^{Surf}\frac{\gamma_{Xe}}{\gamma_H}\frac{\sigma_{\rho XeH}}{s}\alpha^{\frac{r_\pm}{s}}\left[\alpha - \frac{1}{\alpha}\right] \quad (6)$$

at a contact time of $\tau_{cntct} = (2\ln(\alpha))/s$. Here the root of the ratio of the rate matrix eigenvalues is defined by $\alpha \equiv \sqrt{\lambda_-/\lambda_+}$. Assumptions based on the magnitudes of the rates gained experimentally, namely $\rho'_{1\rho Xe} + (\sigma_{\rho XeH}/\theta') \gg \rho_{1\rho H} + \sigma_{\rho XeH}$, can be used to derive an approximate form for the maximum CP enhancement

$$\xi_H^{SS} \approx \frac{\gamma_{Xe}}{\gamma_H}\theta'\xi_{Xe}^{Surface}\left[\frac{\sigma_{\rho XeH}}{\theta'\rho'_{1\rho Xe} + \sigma_{\rho XeH}}\right]. \quad (7)$$

This result is similar to the steady-state SPINOE enhancement (Eq. (5)) with the exception of the functional form of the cross-relaxation term.

3. Experimental

A variety of experiments were performed to characterize the kinetics of polarization transfer for CP experiments. T_1 experiments were performed using conventional methods, and spin-locking experiments were performed to obtain $T_{1\rho}$ values. CP build-up curves as a function of contact time were obtained and cross-relaxation rates were gained from these curves using T_1 and $T_{1\rho}$ data. Hartmann–Hahn curves were obtained to characterize matching conditions. ^{129}Xe NMR adsorption experiments were performed to obtain the xenon surface polarization at different temperatures using previously obtained BET data [25] to calculate the xenon coverage on the silica surface. Complete BET characterization may be seen in L. Smith et al. [25]. SPINOE enhancement experiments were performed for comparative studies.

A continuous flow of hyperpolarized ^{129}Xe was produced by an optical pumping setup described previously in the literature [36]. A cell containing a small amount of Rb metal was held in an insulated oven and heated to create Rb vapor. Optical pumping of the Rb D_1 transition (795 nm) was achieved using a broadband, 25 W

semiconductor diode laser (Optopower) with a nominal linewidth of 2 nm and was brought to the cell via a fiber optic cable. The pumping cell was pressurized to 5 atm with a xenon gas mixture of 2% natural abundance Xe (26% of which is ^{129}Xe), 2% N_2, and 96% He, which was used to pressure broaden the Rb absorption line to ~1 nm. At an oven temperature of 145 °C, approximately 30% of the laser light was absorbed by the Rb vapor. A total gas flow rate of 1 cm^3/s was delivered to the NMR probe using 1/4″ Teflon tubing. The gas mixture was introduced into the sample rotor using a capillary tube that extended through a small hole in the rotor cap [37] with a mean ^{129}Xe polarization of 14%. ^{129}Xe polarization was determined by comparing the HP ^{129}Xe NMR signal to a standard of Xe adsorbed on NaY zeolite. The HP xenon partial pressure in the sample rotor was about 0.02 atm. A variety of flow rates were tested to determine maximum xenon polarization. At low-flow rates, xenon relaxation on the surface limits the xenon surface polarization. At large flow rates, xenon flows through the pumping cell too quickly to allow efficient optical pumping. It was found that a flow rate of 1 cm^3/s gave the largest xenon surface signal; therefore, this flow rate was used for all experiments.

All ^{1}H and ^{129}Xe experiments were performed on a 200 MHz Chemagnetics spectrometer with a Tecmag console using a modified Varian 7 mm CPMAS probe. Variable temperature operation was carried out by precooling the bearing gas in a bath of liquid nitrogen. The bearing gas is delivered to the rotor housing via a Dewared transfer line and is heated in-line to attain the desired temperature. The temperature is monitored with a thermocouple located near the rotor housing and is controlled by a temperature controller (Omega). The controller is capable of maintaining the sample temperature within ±1 °C of the set value and was calibrated using $Pb(NO_3)_2$. All experiments were performed under MAS conditions to achieve a satisfactory signal to noise ratio.

SPINOE experiments were also conducted with the modified Varian 7 mm CPMAS probe. SPINOE experiments were performed by flowing hyperpolarized xenon onto the sample at a rate of approximately 1 cm^3/s. Xenon atoms in contact with a surface could then transfer their polarization to protons through the NOE interaction in the laboratory frame [10]. No radio frequency fields were applied during this transfer process. A proton Bloch decay spectrum was then acquired. Recycle delays of 30 s were typically used, allowing ample time for polarization to transfer from xenon to protons. The xenon was polarized using Rb–Xe spin exchange and employing the same laser pumping station described above.

Experiments involving ^{129}Xe–^{13}C CP were performed with a custom built, single input, double resonance 7 mm CPMAS probe constructed from an old commercial Chemagnetics probe. The double resonance circuit, designed by Haase et al. [38], provides simultaneous excitation of two low-frequency nuclei and is illustrated in Fig. 2. The values of the RF components shown produce two tuned frequencies corresponding to ^{13}C and ^{129}Xe Larmor frequencies of 50.44 and 55.47 MHz, respectively. Roughly half of the power delivered to this probe design is dissipated in the dummy resonance coil. Approximately 400–500 W of RF power was necessary to achieve nutation frequencies of 15–20 kHz at 50 MHz. The probe was made capable of variable temperature operation by introducing the drive and bearing gas directly to the top of the probe through an insulated gas stack. The stack is necessary to protect the bore of the magnet from cold VT gas and contained an additional Teflon tube for the flowing xenon gas mixture. All of the gas lines (bearing, drive, and xenon) were connected to the probe by a press fitting to a Teflon collar attached to the stator. To achieve cold temperatures, both the drive and bearing gases were pre-cooled in a liquid nitrogen bath and were gently warmed by an in-line heating coil located approximately 1.5 m from the top of the probe. Temperature regulation was provided by a thermocouple, located within several cm of the rotor housing, connected to a temperature controller (Omega). The temperature was calibrated with a $Pb(NO_3)_2$ sample, but the temperature could only be regulated to roughly ±15 °C of the set temperature due to the external location of the heater associated with this particular probe.

All proton experiments were performed on a single sample consisting of approximately 25 mg of an M-5 silica sample (Cab-O-Sil, Boston MA) with a surface area of 175 m^2/g. Treatment of the sample involved 12 h of evacuation and dehydration at 500 °C prior to loading. The sample rotor was filled in the N_2 environment of a glove box and had minimal exposure to the atmosphere before being protected in an N_2 environment provided by the spinning gases in the probe. Experiments involving ^{129}Xe–^{13}C CP were performed on 90 mg

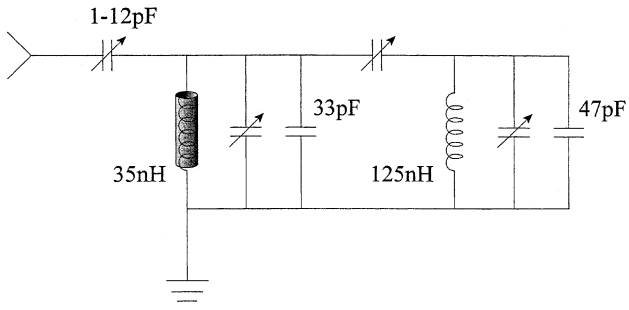

Fig. 2. A schematic of the Haase, Curro, Slichter style single input, double resonance probe circuit [38] used in the ^{129}Xe–^{13}C CP experiments. The illustrated values of the RF components produce two tuned frequencies corresponding to ^{13}C and ^{129}Xe Larmor frequencies of 50.44 and 55.47 MHz, respectively.

of a $^{13}CD_3OD$ methoxylated Cab-O-Sil HS-5 silica sample (300 m^2/g). The silica substrate was pretreated by dehydration at 400 °C for 4 h and was subsequently treated with D_2O to exchange the surface silanol protons with deuterons. Approximately 0.6 mL of D_2O was delivered to 98 mg of silica using a gas rack after a series of three freeze-pump-thaw cycles. The sample was then heated to 140 °C under vacuum for 2 h, cooled to room temperature and evacuated overnight. Methoxylation involved introducing 0.22 mmol of uniformly labeled methanol to 98 mg of the deuterated silica sample and heating for 4 h at 400 °C. Spin counting experiments were used to estimate the methanol coverage, which was determined to be about 25%.

4. Results

4.1. CP mechanism and temperature dependence

A typical ^{129}Xe–^1H CP spectrum for the silanol protons of a fumed silica sample is depicted in Fig. 3a. The spinning sidebands occur from a combination of chemical shift anisotropy and residual dipolar coupling [39]. The CP build-up curve seen in Fig. 3b has the familiar form of growth at a rate characterized by $\sigma_{\rho XeH}$. To probe the nature of the polarization transfer mechanism, a series of Hartmann–Hahn spectra were recorded for ^{129}Xe–^1H CP to surface protons on the fumed silica sample as a function of temperature. Fig. 4 shows the matching conditions under MAS at low (136 K) and high (296 K) temperatures. Although these spectra are broad (FWHM 13.3 and 13.5 kHz, respectively), both have prominent features at the first harmonics of the spinning frequency. This is expected for CP that arises from dipolar coupling under MAS conditions. The CP efficiency improves by approximately ~40% by moving off the matching condition by $\pm\omega_r$, which is where all subsequent CP experiments were performed. The matching conditions are nearly unchanged in going from high to low temperature, with the exception that the high-temperature spectrum has somewhat sharper sideband features. The Hartmann–Hahn curves also contain an on-resonance matching

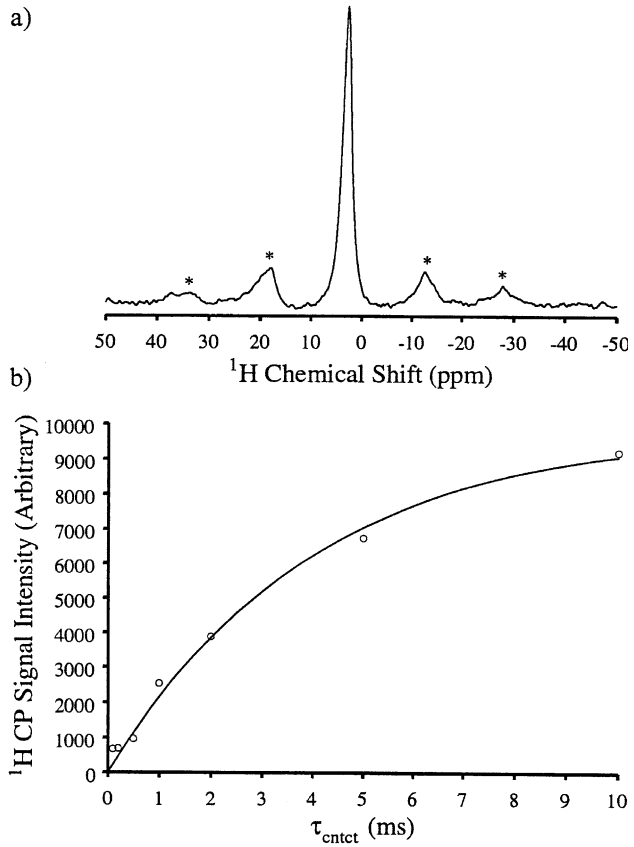

Fig. 3. (a) A typical ^{129}Xe–^1H CPMAS spectrum ($\nu_r \sim 3.3$ kHz) for roughly 25 mg of an M-5 silica sample at $T = 136$ K. A recycle delay of 3 s was used and a total of 16 transients were acquired. Xenon decoupling was not necessary during acquisition. (b) A CP build-up curve obtained by varying the contact time from 0.1 to 10 ms in logarithmic steps, and fit to Eq. (3) in the text.

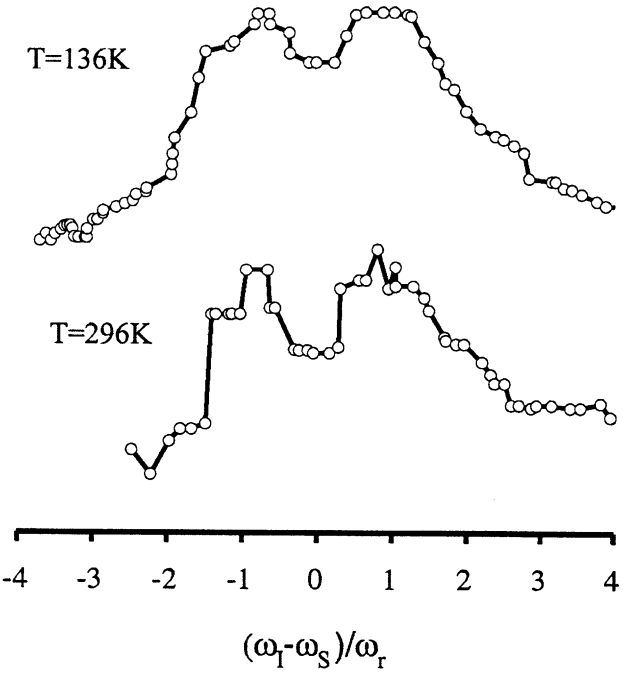

Fig. 4. Hartmann–Hahn matching curves for HP Xe CP to protons on the M-5 silica sample at room (296 K) and cold (136 K) temperatures. The spectra were acquired with the proton B_1 field fixed at a frequency of ~29 kHz, while the power of the xenon channel was incremented/decremented in steps of 0.1 dB from the matching condition. The nutation frequency of the xenon was calibrated at each step using a two-point method developed by Haupt [40]. A three-point box car average was used to smooth the curves, which had some jagged features. The window for the average was chosen to be significantly smaller than the spinning speed (equivalent to 7 pts) to avoid obscuring any sideband features. A CP contact time of 10 ms was used for each point in the spectrum.

condition, which is another indication of dipolar coupling mediated CP, but does not rule out the possibility of J-coupling polarization transfer. However, as previously stated, J-coupling mediated polarization transfer is an unlikely mechanism due to the low-coupling strength predicted to be on the order of mHz–μHz [32].

The temperature dependence of the CP enhancement over the Bloch decay signal is illustrated in Fig. 5. The CP signal is much larger at cold temperatures. Somewhat unexpectedly, HP Xe CP provides polarization transfer to surface nuclei over a large range of temperatures, including those as high as 323 K. The total acquisition times for the CP spectra with good S/N are short (60–90 s), even at high temperatures.

Not surprisingly, Xe adsorption plays a crucial role in the size of the CP signal. In Fig. 6a, xenon spectra are shown as a function of temperature. The adsorbed xenon peak grows dramatically in intensity at colder temperatures, and the chemical shift increases. Though the CP signal is only a fraction of the Bloch decay, the "enhancement" of surface proton magnetization is large when considering the low-xenon surface coverages at the warmer temperatures. Fig. 6b shows the temperature dependence of the scaled xenon surface coverage, θ', as determined by BET isotherm measurements. Near room temperature, coverages are less than 1% but increase dramatically with decreasing temperature, approaching 72% at $T = 136$ K. The ^{129}Xe coverage can be obtained by scaling the total xenon coverage by the isotopic abundance, 26%. The coverage and subsequently the ^{1}H CP signal could be improved by a factor of approximately 3.5 by using isotopically enriched ^{129}Xe. Obviously the magnitude of the xenon spin reservoir is not solely determined by the surface coverage but also by the polarization of the adsorbed xenon. Assuming that the gas phase xenon polarization is roughly temperature independent, surface coverage information can be used to determine the xenon surface polarization by measuring the intensity of the adsorbed xenon signal. The xenon surface polarization is shown in Fig. 6b.

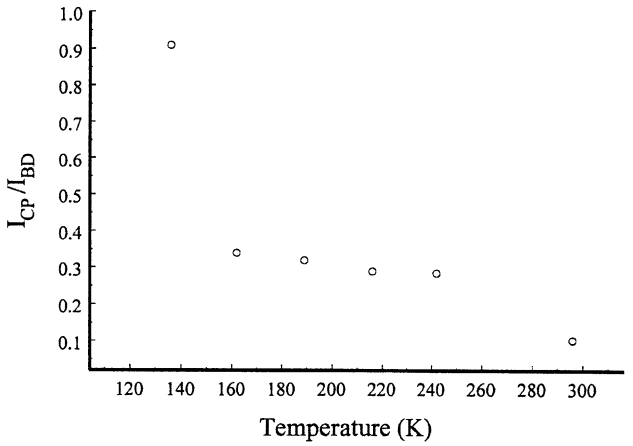

Fig. 5. The temperature dependence of the ^{129}Xe–^{1}H CP enhancement over the Bloch decay signal for the M-5 silica sample. The CP spectrum at each point was acquired using a contact period of 10 ms and was scaled by the number of signal transients relative to the Bloch decay signal.

4.2. Temperature dependence of the relaxation parameters

The decrease in surface polarization of adsorbed xenon with decreasing temperature can be rationalized by longer surface replenishment times evidenced by the effective Xe T_1 data in Fig. 7a. In a simple saturation-recovery experiment, an effective xenon relaxation time, T'_{1Xe}, is measured that is a combination of the true xenon spin-lattice relaxation time, T_{1Xe}, and the rate of xenon loss out of the sample rotor. Since T_1 measurements

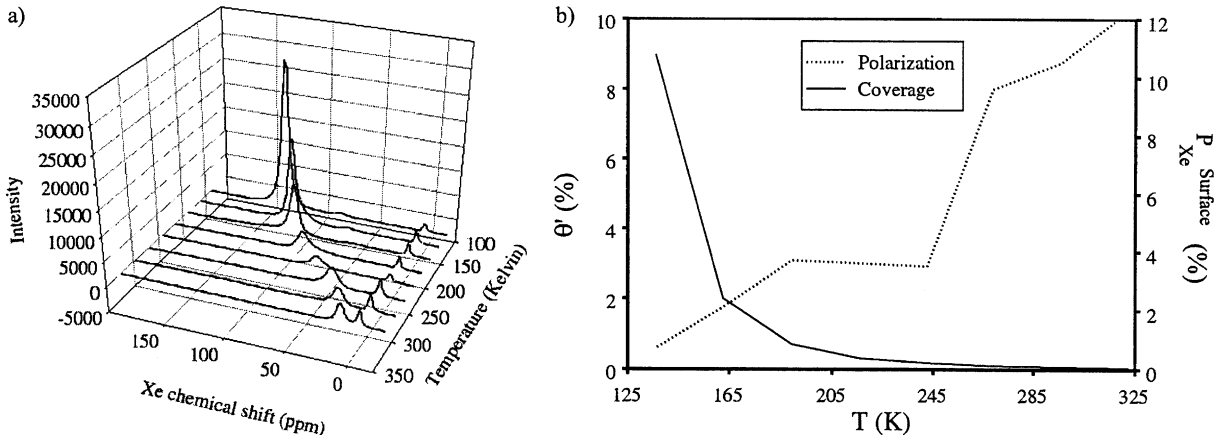

Fig. 6. (a) Plot of xenon spectra at different temperatures. The xenon gas phase peak consistently appears at 0 ppm while the surface adsorbed peak grows in intensity and increases in chemical shift at colder temperatures. (b) The ^{129}Xe surface coverage and polarization on the same sample as a function of temperature. Left and right vertical axes correspond to coverage and polarization, respectively. The coverage has been scaled by the natural isotopic abundance of ^{129}Xe (26%).

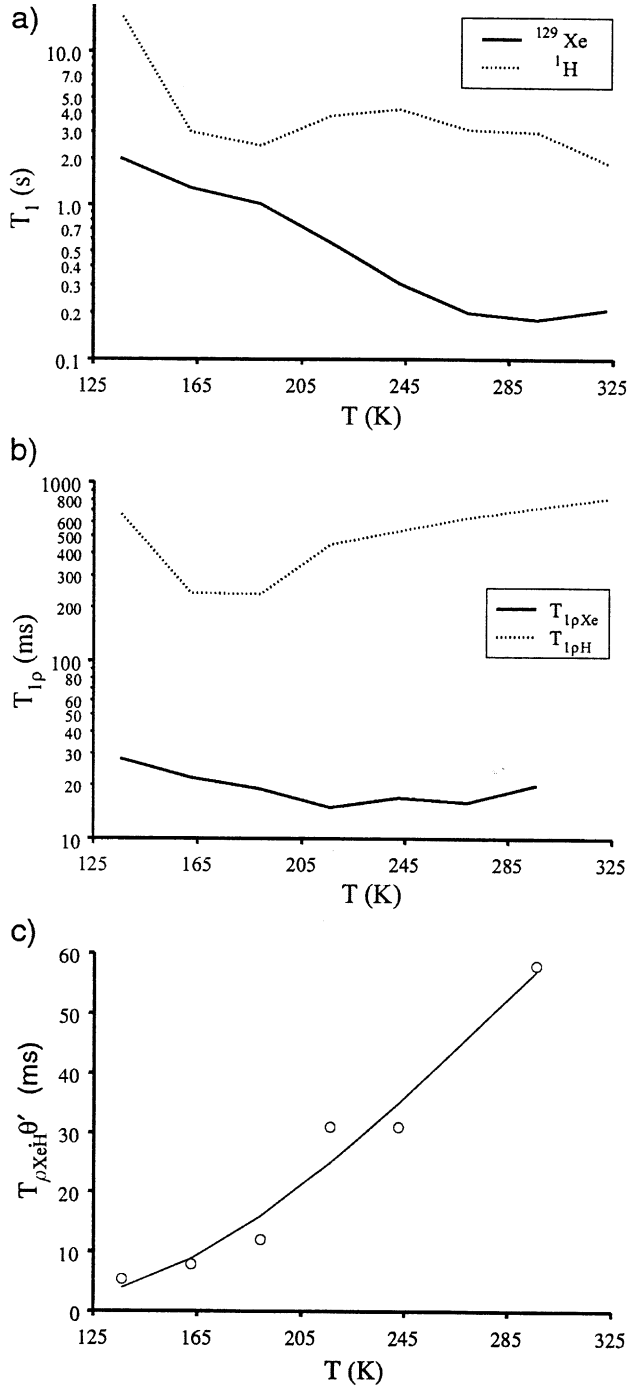

Fig. 7. (a) A semi-log plot of the xenon and proton T_1 relaxation times as a function of temperature for the M-5 silica sample. (b) A semi-log plot of the temperature dependence of the $T_{1\rho}$ relaxation times for adsorbed xenon and surface protons of an M-5 silica sample as measured by a simple spin-locking experiment. (c) The temperature dependence of the coverage-scaled cross-polarization time, $T_{\rho XeH}\theta'$, extracted from CP build up curves using the $T_{1\rho}$ information in Fig. 7b and Eq. (3). The solid line represents an Arrhenius fit to the cross-polarization data, yielding an activation energy of 5.6 kJ/mol.

reflect a return to thermal polarization levels, most of the "T_1 relaxation" rate can be attributed to the xenon loss mechanism, which is a combination of the flow rate and exchange kinetics between the gas and adsorbed phase xenon atoms. Hence, T'_{1Xe} is a measure of the effective surface replenishment time, which becomes dramatically longer at colder temperatures. With longer replenishment times, there is greater auto- and cross-relaxation of the adsorbed xenon and a corresponding drop in the surface polarization. Included for comparison in Fig. 7a are the variable temperature proton T_1 values. Notice that even at the coldest temperatures, the xenon relaxation time is 2–20 times shorter than the corresponding proton T_1.

An inherent limitation to the CP process is spin lattice relaxation in the rotating frame. Fig. 7b illustrates the $T_{1\rho}$ relaxation times for both the surface protons and the adsorbed xenon as a function of temperature. Because of the lower CP sensitivity at high temperatures, $T_{1\rho}$ measurements were made using a simple spin locking experiment rather than indirectly through a CP experiment. Both the xenon and proton data were fit with a bi-exponential function of the form

$$I(\tau_{\mathrm{cntct}}) = C\left(De^{-\frac{\tau_{\mathrm{cntct}}}{T_{1\rho A}}} + (1-D)e^{-\frac{\tau_{\mathrm{cntct}}}{T_{1\rho B}}}\right) \tag{8}$$

to account for rapid decay at short spin lock times. The slower, dominant decay rates for both spins are plotted in Fig. 7b. Considering their relative magnitudes, the ^{1}H $T_{1\rho}$ has little effect on the kinetics of the CP process.

The temperature dependence of the cross-relaxation time, $T_{\rho XeH} = 1/(\sigma_{\rho XeH})$, can be obtained by using the xenon and proton $T_{1\rho}$ information in Fig. 7b as input into Eq. (3) to fit a series of variable temperature CP build up curves. The temperature dependence of $T_{\rho XeH}$ scaled by the xenon coverage is plotted in Fig. 7c. The curve has an exponential form, characteristic of Arrhenius behavior. This behavior can be rationalized by considering a dynamical form of the cross-polarization rate, which is applicable for short correlation times [41]:

$$\sigma_{\rho XeH}(T) = T_{\rho XeH}(T)^{-1} \propto \tau_c(T)M_2(T), \tag{9}$$

where τ_c is the correlation time for the motion that induces cross-relaxation and M_2 is the second moment of the dipolar coupling between the xenon and surface protons. In general, the CP experiment may be divided into three different dynamical regimes, the slow-correlation time regime typically described by a classical thermodynamic picture, the intermediate-correlation time regime, and the fast-correlation time regime (described by the Solomon equations) [42–44]. At cold temperatures, our system is well described by the slow-correlation time picture. At higher temperatures, xenon is extremely mobile on the surface, such that the cross-polarization dynamics can best be described using the short-correlation time theory [44,45], with the CP rate given by Eq. (9). Kolodziejski et al. [44] give conditions ($T_{1\rho Xe} > T_{1\rho H}$ and $(1/T_{1\rho Xe} - 1/T_{1\rho H})^2/4 \gg \sigma_{\rho XeH}\sigma_{\rho HXe}$), where the short-correlation time picture holds and

which are met in our system at higher temperatures, giving evidence to the fact that we are in the short-correlation time regime at higher temperatures. Considering only the temperature-dependent contributions and using the time-averaged second moment given in Eq. (1), the CP time takes the form

$$T_{\rho\mathrm{XeH}}(T)^{-1} \propto \tau_c(T)\frac{\theta'(T)\delta_{\mathrm{site}}}{R^4_{\mathrm{Xe-H}}} \propto \tau_c(T)\theta'(T)$$
$$\Rightarrow T_{\rho\mathrm{XeH}}(T)\theta'(T) \propto \tau_c(T)^{-1}. \quad (10)$$

Eq. (10) indicates that the correlation time is inversely proportional to the product of the cross-polarization time and the scaled xenon surface coverage. When this product is fit with an exponential function, an activation energy of 5.6 kJ/mol is obtained for the xenon motion that induces cross-polarization. In our previous studies of the SPINOE transfer mechanism [25], we proposed a "hopping" model for the motion of adsorbed xenon on a methoxylated silica surface. The hopping activation energy was measured to be 5.4 kJ/mol and is consistent with the result from our CP analysis. However, the correlation time for the motion that gives rise to CP is estimated to be on the order of 10–100 μs, which is much longer than the nanosecond time scale measured for the hopping motion in the SPINOE experiments.

4.3. Comparison of SPINOE and CP

To grasp the value of the CP transfer method, it is useful to compare its temperature dependence to that of the more commonly used SPINOE method of polarization transfer. Fig. 8 shows the enhancements of the CP and SPINOE spectra over the Bloch decay spectrum as a function of temperature. It can be seen that both methods show an increase in enhancement with decreasing temperature; however, CP shows a far more gradual and smaller increase than SPINOE enhancement. Most noticeably, CP provides a measurable amount of polarization transfer over a larger temperature range, including temperatures as high as 323 K. The SPINOE experiment only provides signal enhancement at temperatures below 250 K and only produces larger enhancements than CP for temperatures below 180 K.

Signal averaging plays a large role in determining which method gives the best signal-to-noise ratio within a given amount of time. As stated above, the recycle time in the CP experiment is determined entirely by the adsorbed xenon replenishment rate. Typically, the replenishment time is no longer than 0.1–10 s, but is determined by factors other than the flow rate, including sample packing and rotor geometry. Due to low coverage at high temperatures, the replenishment rate is usually much faster than the T_1 relaxation rate of the surface nuclei as illustrated in Fig. 7a. CP has the added benefit that, due to $T_{1\rho}$ effects, the actually contact time is relatively short (10 ms) and only a portion of the xenon polarization is used during an experiment. The remainder can therefore, be stored along the B_0 field direction after acquisition for a further reduction in the optimal recycle period. SPINOEs, on the other hand, are optimal when allowed to develop over several laboratory frame T_1 periods for the nucleus of interest. In the case of protons on M-5 silica, the effects of the different recycle period requirements for the CP and SPINOE experiments are reflected in the CP signal-to-noise per unit time relative to the Bloch decay signal plotted in Fig. 9. The values of the plotted function were computed by multiplying the measured S/N for the CP experiment by the ratio of the ^{1}H and ^{129}Xe relaxation times. When these factors are considered, the

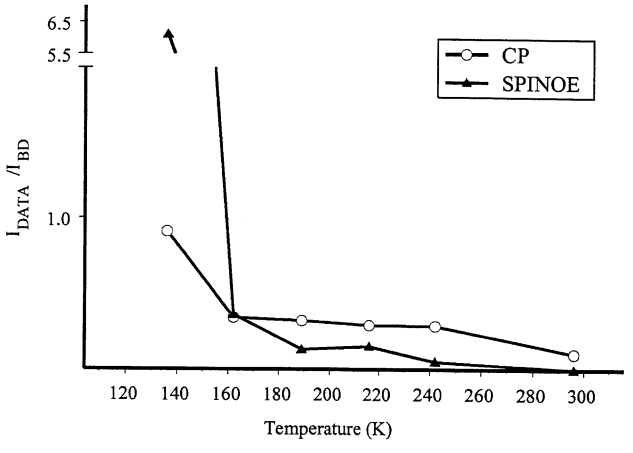

Fig. 8. A comparison of CP enhancement (CP intensity divided by Bloch Decay) with SPINOE enhancement (SPINOE intensity divided by Bloch Decay) for M-5 silica as a function of temperature.

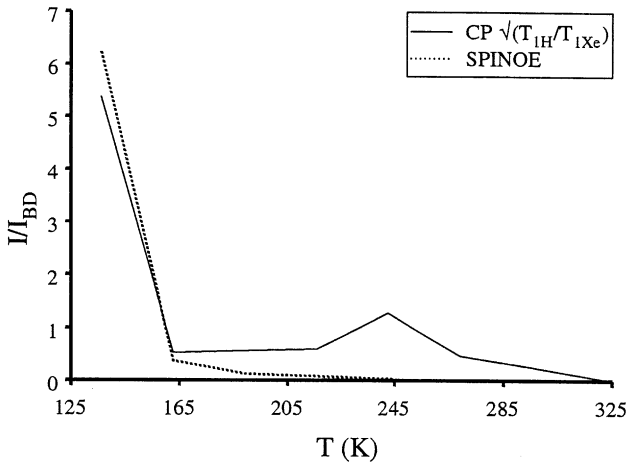

Fig. 9. The temperature dependence of the CP and SPINOE ^{1}H signal-to-noise enhancements relative to the Bloch decay signal. The CP signal is scaled by the root of the ratio of the relevant T_1's for the CP and BD experiments because of the additional time savings available in the CP experiment.

low-temperature performance of both techniques is very comparable.

One of the main reasons for the different temperature behavior in the CP and SPINOE experiments is the different size and behavior of the cross-relaxation rates. Fig. 10 shows the temperature dependence of the cross-relaxation rates for the CP and SPINOE experiments in this study. In addition, we have added the coverage as a function of temperature, as well as data from [25] on the cross-relaxation between Xe and H for a methoxylated silica surface. There are several interesting points that can be made about the data presented in this figure. First, it is evident that the CP cross-relaxation rate is much higher than that for the SPINOE experiment. This is not surprising in that the CP relies on a direct dipolar coupling mechanism proportional to $\gamma_1\gamma_2/r^3$, where as SPINOE acts through the second-order nuclear relaxation process associated with the nuclear Overhauser effect given by terms proportional to $\gamma_1^2\gamma_2^2/r^6$ [46]. In addition, the SPINOE xenon–proton cross-relaxation rates for both the hydroxy and methoxy silica surfaces are very similar. Large uncertainty in the measured values at the warmer temperatures is probably responsible for deviations from the trends observed. It is also evident in this figure that the cross-relaxation terms all show significant temperature dependences. The effect of coverage, and its temperature dependence can also be seen. It is apparent that the coverage contributes in a substantial way to the temperature dependence of the measured cross-relaxation rates. However, coverage does not account for all of that dependence, and the surface dynamics associated with the temperature-dependent value of the correlation time (τ_c) certainly play a role, as we have discussed previously [25]. The large difference in the variable temperature performance of the CP and SPINOE techniques we observed in this study (see Fig. 8), however, does not result primarily from the observed temperature dependences seen in Fig. 10. Instead it derives from the explicit form of the cross-relaxation functional dependences shown in Eqs. (5) and (7). Because the SPINOE scales linearly with the ratio of cross and self-relaxation, the enhancement drops off quickly at higher temperatures where the cross-relaxation rate decreases dramatically. In the CP experiment, however, a similar relative decrease in the cross-polarization rate has a much more modest effect on the enhancement because of the non-linear functional dependence.

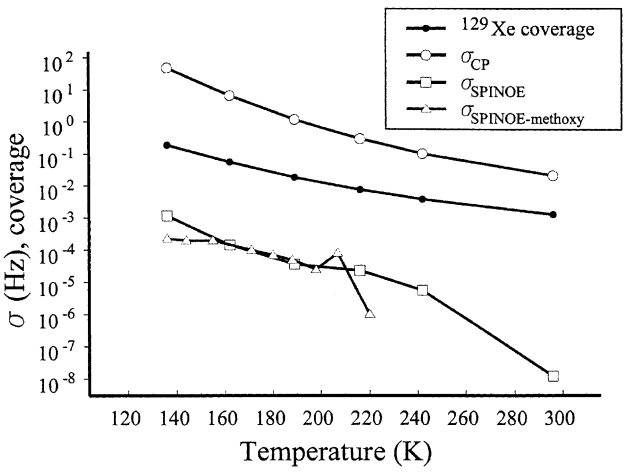

Fig. 10. A comparison of Xe–H cross-relaxation rates measured for different systems of M-5 silica. CP cross-relaxation rates ($\sigma_{\rho XeH}$) were obtained using CP build up curves (see Fig. 7c). SPINOE cross-relaxation rates (σ_{XeH}) were obtained using T_1 information and Eq. (5). SPINOE cross-relaxation rates from Xe to H on adsorbed methoxy groups were obtained from the literature [25]. The temperature dependence of coverage is also given.

From the equations for the steady-state SPINOE (7) and maximum CP enhancements (6) and the data in Fig. 6b, it is apparent that a principal limitation to the high-temperature performance of both techniques is low-surface coverage, and at low temperatures, the diminished surface polarization. The product $(\gamma_{Xe}/\gamma_H)\theta'\varsigma_{Xe}^{Surface}$ represents the absolute maximum polarization enhancement that can be attained by the surface protons in the CP experiment. The potential enhancement ranges from about 3 to 50 times the Bloch decay signal for temperatures between 323 and 136 K. However, the experimentally achieved enhancement only ranges from 0.1 to 0.9 times the Bloch decay (see Fig. 8). The difference is only partly due to the small value of the bracketed term in Eq. (7) at warm temperatures. One possible explanation for the small observed enhancements is that only a small fraction of Xe atoms successfully transfer polarization to surface protons. At the colder temperatures, this effect is more pronounced and may indicate that xenon surface dynamics or possibly insufficient surface wetting could play a role in reducing access of the xenon to surface protons and thereby reducing the polarization transfer. More detailed studies of the selectivity of xenon polarization transfer are required to resolve some of these issues. The cross-polarization dynamics at different temperatures can be compared by calculating the expected signal enhancement as a function of contact time and temperature using Eq. (3), the values for the auto- and cross-relaxation times, and the surface polarization. As shown in Fig. 11, this results in a series of CP buildup and decay curves that show a large temperature dependence in the maximum value due primarily to coverage. In addition, the decay time, largely determined by the xenon $T_{1\rho}$ is significantly shortened at the lower temperatures. As a result, the maximum possible enhancement is reached within a 10 ms contact time below 190 K. It is important to note, however, that the largest enhancement observed was only 0.9 at 136 K indicating that there is a major discrepancy in the predicted and observed enhancements. We believe this is due to selectivity in the xenon polarization transfer.

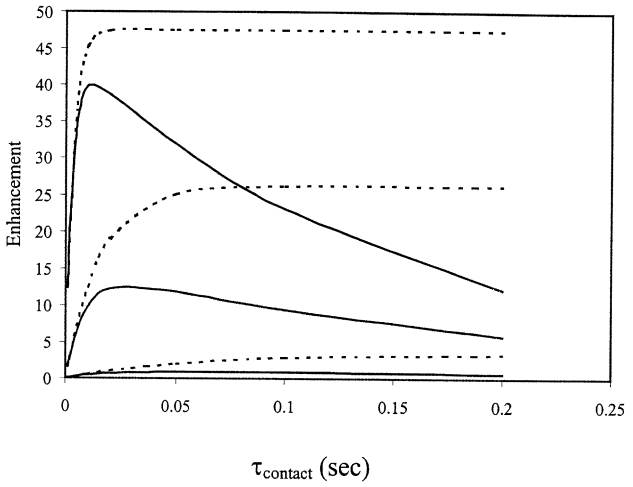

Fig. 11. A graph of theoretical enhancements of CP at different contact times. The solid lines represent the maximum enhancement obtained from Eq. (3), while the dotted lines represent the absolute maximum enhancement obtained by setting $T_{1\rho Xe}$ and $T_{1\rho H}$ to zero. Experiments to determine the values used in these calculations were performed on M-5 silica and are described in the text. Experimentally obtained enhancements were substantially smaller.

4.4. CP surface selectivity

We also investigated the selectivity of CP between surface protons and protons at or near the surface. Depending on the experiment, spin diffusion can spread polarization that is initially transferred to surface nuclei to other sites that are not directly accessible by the xenon gas. To investigate the selectivity in the polarization transfer process, we studied the ^{1}H line shape of the dehydrated fumed silica sample produced in a standard Bloch decay experiment and compared it to the corresponding CP and SPINOE spectra. Previous studies of similar materials [31,47] have identified a variety of proton species including isolated silanol groups located in interparticle regions (1.8–2.1 ppm), silanol groups in rapid exchange with adsorbed water (2.7–4.6 ppm), and bridging silanol groups with weak and strong hydrogen bonding interactions (~5 ppm). The chemical shift range of the hydrated silanol groups has been shown to scale with the hydration level, having a minimum of 2.7 ppm when completely dehydrated and a maximum of 4.6 ppm in the limit of total surface saturation [47]. The Bloch decay spectrum of our silica sample consists of a large, asymmetric peak with a maximum at 1.7 ppm and a shoulder at ~2.2–2.9 ppm. We attribute the peak at 1.7 ppm to isolated silanol protons, while the downfield shoulder has been assigned to silanols in exchange with a very low coverage of adsorbed water (<5% coverage). Our silica sample may have been contaminated with a small amount of water due to brief atmospheric exposure during sample loading.

Fig. 12a shows the ^{1}H spectra for M-5 silica produced by Bloch decay, spin-locked Bloch decay, SPINOE and CP experiments at a temperature of 136 K. Most noticeably, the proton spectra are nearly identical with the exception of the CP spectrum, which shows a more downfield peak at 2.9 ppm. To ensure that the difference between the CP and Bloch decay lineshapes was not due to $T_{1\rho}$ effects, an additional spectrum is shown in Fig. 12b corresponding to a Bloch decay experiment followed by a spin-locking period equivalent to the contact pulse in the CP experiment. The strong similarity between the spin locked and Bloch decay spectra indicates that $T_{1\rho}$ relaxation during the 10 ms contact time has no serious effect on the ^{1}H lineshape. The discrepancy between the CP and Bloch decay lineshapes can be attributed to the selectivity in the polarization transfer process. The isolated silanols located in inter-particle regions have been shown to be inaccessible to adsorbed

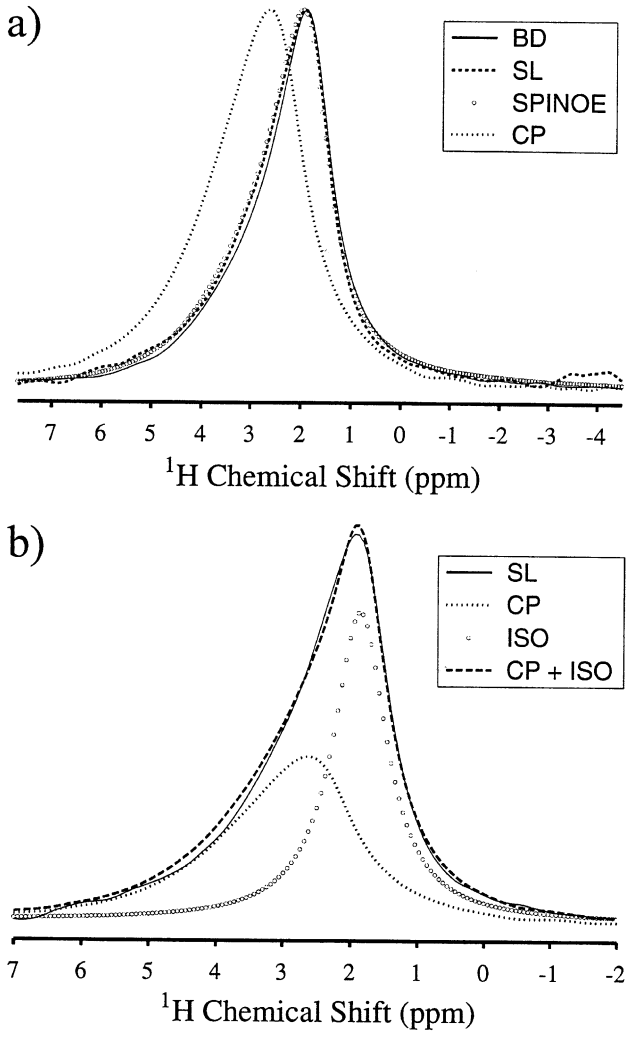

Fig. 12. (a) A comparison of the M-5 silica proton lineshapes produced by Bloch decay, spin-locked Bloch decay, SPINOE and HP Xe CP experiments at 136 K. The lineshapes are nearly identical with the exception of the CP spectrum. (b) An illustration of the decomposition of the Bloch decay lineshape into hydrated and isolated silanol components using the CP lineshape.

water [31,47]. The similarity in size between water molecules and xenon atoms would suggest that these sites may also be inaccessible to adsorbed xenon. Using the CP lineshape as a model for the hydrated silanol resonance and an additional Lorentzian function to represent isolated silanols, the Bloch decay spectrum can be deconvoluted into the separate resonances. Fig. 12b shows that the Bloch decay lineshape is well described by the combination of the CP lineshape and the additional Lorentzian line.

The lineshape analysis described above makes it possible to estimate the fraction of the silica protons that are not accessible in the CP experiment. Maciel et al. [31] estimated the fraction of isolated silanol groups in fumed silica to be as high as 30–50% based on particle size and coordination. Table 1 shows the results of the lineshape analysis for the range of temperatures used in this study. The average fraction of isolated silanol groups was found to be 40%, consistent with previous studies. The average hydrated and isolated silanol shifts were found to be 2.5 and 1.7 ppm, respectively, which are also consistent with previously reported proton shifts for fumed silica in the dehydration limit [47].

The similarity between the SPINOE and Bloch decay spectra can most likely be attributed to spin diffusion. Unlike CP, in which the polarization transfer occurs over a time period determined by the cross-polarization time (~10 ms), SPINOE enhancements are built up over several surface nuclear T_1 periods. The resulting SPINOE periods are on the order of 1–100 s and are therefore, more susceptible to spin diffusion.

4.5. CP to an X nucleus

Most materials with interesting surface properties are composed of atoms other than protons. An obvious extension of the hyperpolarized Xe CP experiment is to investigate low-frequency nuclei with inherently low sensitivity. A special double-resonance probe was constructed for low-frequency CP experiments. To investigate ^{129}Xe–^{13}C CP, which has a resonance frequency difference of only 5 MHz at 4.7 T. The circuit design shown in Fig. 2, originally proposed by Haase et al. [38] and similar to that of Reimer et al., [48] was used to perform the low-frequency double resonance experiment using only a single X channel. To demonstrate the feasibility of HP Xe CP to lower-frequency nuclei, we incorporated this circuit into a commercial 7 mm Chemagnetics CPMAS probe to observe cross-polarization from hyperpolarized xenon to the ^{13}C nuclei of a labeled, methoxylated silica sample.

Fig. 13 shows the Bloch decay, SPINOE and HP Xe CP signals for the deuterated-methoxylated silica sample at 293 and ~143 K. Again, at high temperatures, only CP provided any surface signal enhancement, while both CP and SPINOE provided enhancements at a temperature of ~143 K. Unlike the case of protons in M-5 silica, the ^{13}C CP and SPINOE spectra for the methoxylated HS-5 silica are very similar in shift at 49.6 and 49.7 ppm, respectively. Both xenon-enhanced spectra are shifted downfield from the BD resonance at 47.6 ppm. There are several possible explanations for the differences in these spectra. For example, the sample could contain both methoxy groups and physisorbed methanol on the surface. Shifts between chemisorbed and physisorbed species have been reported extensively in catalysis studies. In this case, CP and SPINOE from HP Xe may selectively enhance the more rigid methoxy groups. Another possibility is that the intense heating during sample preparation allows methanol molecules to access the isolated silanols groups, coating these sites with methoxy groups. Once cooled, these sites again become inaccessible and the CP and SPINOE experiments only reflect enhancements of the accessible sites. Unlike the case of protons on silica, the methoxy coverage is too low and the dipolar coupling between groups too weak to promote efficient spin diffusion. Hence the CP and SPINOE spectra share similar lineshapes.

Table 1
A table of peak positions, δ, and linewidths, Γ, of the hydrated (H_2O) and isolated (iso) silanol resonances produced by applying the deconvolution procedure illustrated in Fig. 12b to the variable temperature Bloch decay data. The table also contains the fraction of the total proton lineshape corresponding to isolated silanols, X_{iso}

T (K)	X_{iso}	δ_{iso} (ppm)	Γ_{iso} (Hz)	$\delta_{hydrated}$ (ppm)	$\Gamma_{hydrated}$ (Hz)
323	0.4	1.6	318	2.7	623
296	0.4	1.5	165	2.3	496
269	0.4	1.6	206	2.5	530
242	0.4	1.7	174	2.5	591
216	0.3	1.6	150	2.2	527
189	0.4	1.8	147	2.4	561
162	0.3	1.8	126	2.2	530
136	0.6	1.9	208	2.9	491
Average	0.4	1.7	187	2.5	544

Silanol peak information.

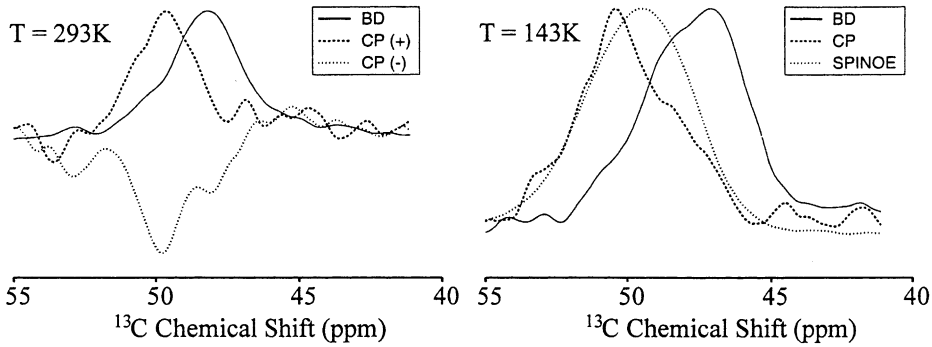

Fig. 13. The ^{13}C Bloch decay, SPINOE and HP Xe CP spectra for a ^{13}C labeled, methoxylated HS-5 silica sample at room (293 K) and cold (~143 K) temperatures. At room temperature, no SPINOE was observed. The CP(+) and CP(−) spectra correspond to experiments using xenon polarized anti-parallel and parallel to the B_0 field, respectively, and are included for purpose of verification.

A table of ^{13}C chemical shifts, linewidths and sensitivity enhancements is given in Table 2. At $T \sim 143$ K, the SPINOE gave a significant signal enhancement, 770%, but the CP never produced signal enhancements greater than 40%. The CP signal intensity varied between 5–40% of the Bloch decay and was difficult to measure accurately at cold temperatures because of large temperature fluctuations in our variable temperature setup. A possible explanation for the poor performance of the CP mechanism on this sample can be made based on the dipolar coupling strength. According to our previous studies of ^{13}C SPINOEs [25], the average xenon–carbon distance on methoxylated silica is 3.6 Å, compared to 2.5–3.0 Å expected for the protons on bare HS-5 silica. Assuming that the major difference in the cross-polarization times for ^{1}H on silica and ^{13}C on the methoxylated silica sample is due to the dipolar coupling strength, one could expect CP times that are nearly 150 times longer than those displayed in Fig. 7c. Even at the coldest temperatures, the CP time could easily reach in excess of 1 s. Short xenon $T_{1\rho}$'s limit the optimal contact times and greatly reduce the ability to CP to nuclei with such large internuclear distances to the adsorbed xenon atoms. Fortunately, the xenon–carbon mean separation distance is due in part to the geometry of the attached methanol group and is not necessarily an inherent limitation to lower-frequency nuclei HP Xe CP. With direct contact between the adsorbed xenon and low-frequency nuclei, contact times are only expected to be about 40 times longer than for the silica protons, keeping CP times down to roughly 150 ms at cold temperatures. An obvious extension of these experiments will be to incorporate a triple resonance probe and spectrometer to carry out HP Xe–^{1}H–X double-CP experiments. Such experiments are currently being planned.

5. Conclusions

Cross-polarization from HP Xe to surface nuclei is a robust method for obtaining surface-selective NMR spectra for a variety of materials and over a wide temperature range. Although the materials in this fundamental study were primarily limited to simple silica surfaces, proton enhancements using HP Xe CP have been observed in both microporous and mesoporous materials including acid sites and adsorbates in zeolites [30], protons on polymer surfaces [9,26], and silane groups in porous silicon [49]. Hartmann–Hahn spectra provide the first conclusive evidence that the polarization transfer in the HP Xe CP experiment is mediated by a through-space dipolar coupling between the adsorbed xenon and the surface nuclei. A simple model for the time-averaged coupling correctly predicts the coverage dependence of the observed cross-polarization rates. From these rates, the Arrhenius dependence of the correlation time yields an activation energy for surface

Table 2
A table of ^{13}C peak positions, δ, and linewidths, Γ, for the methoxylated silica produced by the BD, SPINOE, and CP experiments illustrated in Fig. 13. The last column in the table gives the signal-to-noise per scan for each experiment as a percentage of the Bloch decay spectrum

T (K)	Spectrum	δ (ppm)	Γ (Hz)	I/I_{BD} (%)
293	BD	48.3	105	100
	CP(+)	49.2	138	3
	CP(−)	49.5	143	−3
143	BD	47.6	132	100
	CP	49.6	138	<40
	SPINOE	49.7	110	776

^{13}C Methoxylated silica information.

xenon diffusion similar to that observed in studies of the SPINOE mechanism on similar silica surfaces, lending support for a xenon "hopping" motion model.

The principal limitation to the sensitivity enhancement provided by HP Xe CP appears to be the adsorbed xenon steady-state polarization density. At warmer temperatures, the surface xenon polarization is nearly as large as the gas phase polarization, but coverage is low. While the coverage can be increased up to and exceeding one monolayer at colder temperatures, the xenon replenishment rate decreases resulting in a dramatic decrease in the surface xenon polarization. Temperatures colder than those studied could not be used because xenon freezes on the surface, pushing the xenon replenishment rate to approximately zero. Low-surface xenon polarization could be partially compensated by the use of larger laser powers to polarize a higher percentage of xenon. It will also be less of a problem when investigating samples with lower-surface area. The relative magnitudes of the CP rate and the $T_{1\rho}$ relaxation rate also play a key role in determining the maximum signal enhancement. Ultimately, weak dipolar couplings and short $T_{1\rho Xe}$'s further limit the magnitude of the HP Xe CP signal. Finally, measurements at cold temperatures indicate that only a fraction of the xenon lineshape contributes to CP process. Further studies are needed to determine what parameters affect selectivity among the xenon for transferring their polarization.

Unlike the SPINOE experiment, which is limited to cold (<250 K) temperatures and samples with ideal relaxation properties, the CP technique has been used successfully to probe materials at temperatures above room temperature, samples with surface areas as small as $5\,m^2/g$, and materials with short (<1 s) T_1 relaxation times. However, the differences between CP and SPINOE outlined in this study suggest that the two techniques can provide complementary information. SPINOE provides significantly larger enhancements at temperatures below 160 K, while CP performs well at warm temperatures and is more selective to surface nuclei. CP has the additional advantage of short acquisition delays and can easily be incorporated into 2D NMR experiments [30].

The ^{129}Xe–^{13}C CP experiment on the methoxylated silica sample demonstrates that the technique can be used to enhance low-frequency nuclei selectively and will hopefully provide useful surface information on a wide variety of samples. To achieve this goal in a practical amount of time, higher-xenon polarizations are necessary, but should be attainable. Polarization during continuous flow inside our optical pumping cell has been estimated to be as high as 40%, nearly 2.5 times the gas phase polarization delivered to the sample. If such an increase can be delivered to the surface xenon polarization, the acquisition time for low frequency, room temperature CP spectra could be as short as 10–15 min.

Acknowledgments

J.S. thanks the Purdue Research Foundation for graduate support. This work was supported by the NSF (CHE01-09626), the donors of the Petroleum Research Fund, and Alfred P. Sloan Foundation.

References

[1] T.G. Walker, W. Happer, Spin-exchange optical pumping of noble-gas nuclei, Rev. Mod. Phys. 69 (1997) 629, and references therein.
[2] B.M. Goodson, Nuclear magnetic resonance of laser-polarized noble gases in molecules, materials, and organisms, J. Mag. Res. 155 (2002) 157.
[3] T. Pietrass, NMR of molecules and surfaces using laser-polarized xenon, Colloids and Surfaces A. 158 (1999) 51.
[4] C.I. Ratcliffe, Xenon NMR, Ann. R. NMR S. 36 (1998) 123.
[5] R. Tycko, J.A. Reimer, Optical pumping in solid-state nuclear magnetic resonance, J. Phys. Chem. 100 (1996) 13240.
[6] D. Raftery, B.F. Chmelka, Xenon NMR Spectroscopy, in: B. Blumich, R. Kosfeld (Eds.), NMR Basic Principles and Progress, vol. 30, Springer-Verlag, Berlin, 1994, p. 111.
[7] C.R. Bowers, H.W. Long, T. Pietrass, H.C. Gaede, A. Pines, Cross-polarization from laser-polarized solid xenon to $^{13}CO_2$ by low-field thermal mixing, Chem. Phys. Lett. 205 (1993) 168.
[8] B. Driehuys, G.D. Cates, W. Happer, H. Mabuchi, B. Saam, M.S. Albert, A. Wishnia, Spin transfer between laser-polarized ^{129}Xe nuclei and surface protons, Phys. Lett. A 184 (1993) 88.
[9] H.W. Long, H.C. Gaede, J. Shore, L. Reven, C.R. Bowers, J. Kritzenberger, T. Pietrass, A. Pines, P. Tang, J.A. Reimer, High-field cross-polarization NMR from laser-polarized xenon to a polymer surface, J. Am. Chem. Soc. 115 (1993) 8491.
[10] G. Navon, Y.-Q. Song, T. Rõõm, S. Appelt, R.E. Taylor, A. Pines, Enhancement of solution NMR and MRI with laser-polarized xenon, Science 271 (1996) 1848.
[11] D. Raftery, H. Long, T. Meersmann, P.J. Grandinetti, L. Reven, A. Pines, High-field NMR of adsorbed xenon polarized by laser pumping, Phys. Rev. Lett. 66 (1991) 584.
[12] R.J. Fitzgerald, K.L. Sauer, W. Happer, Cross-relaxation in laser-polarized liquid xenon, Chem. Phys. Lett. 284 (1998) 87.
[13] S. Appelt, F.W. Haesing, S. Baer-Lang, N.J. Shah, B. Blumich, Proton magnetization enhancement of solvents with hyperpolarized xenon in very low-magnetic fields, Chem. Phys. Lett. 348 (2001) 263.
[14] M. Haake, B.M. Goodson, D.D. Laws, E. Brunner, M.C. Cyrier, R.H. Havlin, A. Pines, NMR of supercritical laser-polarized xenon, Chem. Phys. Lett. 292 (1998) 686.
[15] J.C. Leawoods, B.T. Saam, M.S. Conradi, Polarization transfer using hyperpolarized, supercritical xenon, Chem. Phys. Lett. 327 (2000) 359.
[16] M. Luhmer, B.M. Goodson, Y.-Q. Song, D.D. Laws, L. Kaiser, M.C. Cyrier, A. Pines, Study of xenon binding in cryptophane-A using laser-induced NMR polarization enhancement, J. Am. Chem. Soc. 121 (1999) 3502.
[17] T. Rõõm, S. Appelt, R. Seydoux, E.L. Hahn, A. Pines, Enhancement of surface NMR by laser-polarized noble gases, Phys. Rev. B. 55 (1997) 11604.
[18] D. Raftery, E. MacNamara, G. Fisher, C.V. Rice, J. Smith, Optical pumping and magic angle spinning: Sensitivity and resolution enhancement for surface NMR obtained with laser-polarized xenon, J. Am. Chem. Soc. 119 (1997) 8746.
[19] E. Brunner, R. Seydoux, M. Haake, A. Pines, J.A. Reimer, Surface NMR using laser-polarized ^{129}Xe under magic angle spinning conditions, J. Magn. Reson. 130 (1998) 145.

[20] E. Brunner, M. Haake, A. Pines, J.A. Reimer, R. Seydoux, Enhancement of ^{13}C NMR signals in solid C_{60} and C_{70} using laser-polarized xenon, Chem. Phys. Lett. 290 (1998) 112.
[21] T. Pietrass, R. Seydoux, A. Pines, Surface selective $^{1}H/^{29}Si$ CP NMR by NOE enhancement from laser polarized xenon, J. Magn. Reson. 133 (1998) 299.
[22] E. MacNamara, G. Fisher, J. Smith, C.V. Rice, S.-J. Hwang, D. Raftery, Cross-polarization and cross-relaxation from laser-polarized xenon to surface species, J. Phys. Chem. B. 103 (1999) 1158.
[23] R. Seydoux, A. Pines, M. Haake, J.A. Reimer, NMR with a continuously circulation flow of laser-polarized ^{129}Xe, J. Phys. Chem. B. 103 (1999) 4629.
[24] E. MacNamara, C.V. Rice, J. Smith, L.J. Smith, D. Raftery, Cross-relaxation dynamics between laser-polarized xenon and a surface species using a simple three-spin model, Chem. Phys. Lett. 317 (2000) 165.
[25] L.J. Smith, J. Smith, E. MacNamara, K. Knagge, D. Raftery, Variable temperature study of the cross-relaxation dynamics in the hyperpolarized xenon-induced enhancement of surface nuclei, J. Phys. Chem. B. 105 (2001) 1412.
[26] H.C. Gaede, Y.-Q. Song, R.E. Taylor, E.J. Munson, J.A. Reimer, A. Pines, High-field cross-polarization NMR from laser-polarized xenon to surface nuclei, Appl. Magn. Reson. 8 (1995) 373.
[27] J.A. Ripmeester, Nuclear shielding of trapped xenon obtained by proton-enhanced, magic-angle spinning ^{129}Xe NMR spectroscopy, J. Am. Chem. Soc. 104 (1982) 289.
[28] F. Lee, J.E. Gabe, J.S. Tse, J.A. Ripmeester, Crystal structure, CP/MAS ^{129}Xe, and ^{13}C NMR of local ordering in Dianins compound clathrates, J. Am. Chem. Soc. 110 (1988) 6014.
[29] M. Mansfeld, W.S. Veeman, ^{1}H–^{129}Xe double resonance NMR in a polymer blend, Chem. Phys. Lett. 222 (1994) 422.
[30] J. Smith, L.J. Smith, K. Knagge, E. MacNamara, D. Raftery, Hyperpolarized xenon-mediated cross-polarization to material surfaces observed at room temperature and above, J. Am. Chem. Soc. 123 (2001) 2927.
[31] C.C. Liu, G.E. Maciel, The fumed silica surface: A study by NMR, J. Am. Chem. Soc. 118 (1996) 5103.
[32] F.R. Salsbury, R.A. Harris, Estimation of the Fermi contact contribution to the xenon–hydrogen and xenon–xenon spin–spin coupling constants, Mol. Phys. 94 (1998) 307.
[33] M. Mehring, Principles of High-Resolution NMR in Solids, Second ed., Springer-Verlag, Berlin, 1983.
[34] E.A. Flood, The Solid-Gas Interface, Marcel Dekker, New York, 1967.
[35] L. Muller, A. Kumar, T. Baumann, R.R. Ernst, Transient oscillations in NMR cross-polarization experiments in solids, Phys. Rev. Lett. 32 (1974) 1402.
[36] B. Driehuys, G.D. Cates, E. Miron, K. Sauer, D.K. Walter, W. Happer, High-volume production of laser-polarized ^{129}Xe, Appl. Phys. Lett. 69 (1996) 1668.
[37] M. Hunger, T. Horovath, A new MAS NMR probe for in-situ investigations of hydrocarbon conversion on solid catalysts under continuous-flow conditions, J. Chem. Soc. Chem. Commun. 14 (1995) 1423.
[38] J. Haase, N.J. Curro, C.P. Slichter, Double resonance probes for close frequencies, J. Mag. Reson. 135 (1998) 273.
[39] D.P. Burum, W.K. Rhim, An improved NMR technique for homonuclear dipolar decoupling in solids: Application to polycrystalline ice, J. Chem. Phys. 70 (1979) 3553.
[40] E. Haupt, A timesaving method to determine the length of a 90° pulse, J. Mag. Reson. 49 (1982) 358.
[41] E.O. Stejskal, J.D. Memory, High-Resolution NMR in the Solid State, Oxford University Press, Oxford, 1994.
[42] C. Fulber, D.E. Demco, B. Blumich, The influence of molecular motion on cross-polarization in cross-linked elastomers, Solid State NMR 6 (1996) 213.
[43] W. Koloziejski, J. Klinowski, Kinetics of cross-polarization in solid-state NMR: A guide for chemists, Chem. Rev. 102 (2002) 613.
[44] W. Kolodziejski, A. Corma, K. Wozniak, J. Klinowski, $^{13}C \rightarrow {}^{1}H$ cross-polarization NMR in solids at natural ^{13}C abundance, J. Phys. Chem. 100 (1996) 7345.
[45] D. Schulze, H. Ernst, D. Fenzke, W. Meiler, H. Pfeifer, Applicability of the NMR cross-polarization technique to separate rigid and mobile components in coal structure, J. Phys. Chem. 94 (1990) 3499.
[46] J.H. Noggle, The Nuclear Overhauser Effect, Chemical Applications, Academic Press, New York, 1971.
[47] J.-B. DEspinose de la Caillerie, M.F. Aimeur, Y. El Kortobi, A.P. Legrand, Water adsorption on pyrogenic silica followed by H-1 MAS NMR, J. Colloid Interface Sci. 194 (1997) 434.
[48] S. Hu, J.A. Reimer, A.T. Bell, Single-input double-tubed circuit for double resonance nuclear magnetic resonance experiments, Rev. Sci. Instrum. 69 (1998) 477.
[49] In preparation.